

Dark matter in Draco and the Local Group: Implications for direct detection experiments

Ben Moore* and Carlos Calcáneo-Roldán

Department of Physics, Durham University, Science laboratories, Durham, DH1 3LE, UK.

Joachim Stadel, Tom Quinn, George Lake and Sebastiano Ghigna

Department of Astronomy, University of Washington, Seattle, WA 98195, USA

Fabio Governato

Osservatorio Astronomico di Brera, via Bianchi 46, Merate, Italy

(October 26, 2018)

We use a cosmological simulation of the Local Group to make quantitative and speculative predictions for direct detection experiments. Cold dark matter (CDM) halos form via a complex series of mergers, accretion events and violent relaxation which precludes the formation of significant caustic features predicted by axially symmetric collapse. The halo density profiles are combined with observational constraints on the galactic mass distribution to constrain the local density of cold dark matter to lie in the range $0.18 \lesssim \rho_{CDM}(R_{\odot})/(\text{GeV cm}^{-3}) \lesssim 0.30$. In velocity space, coherent streams of dark matter from tidally disrupted halos fill the halo and provide a tracer of the merging hierarchy. The particle velocities within triaxial CDM halos cannot be approximated by a simple Maxwellian distribution and is radially biased at the solar position. The detailed phase space structure within the solar system will depend on the early merger history of the progenitor halos and the importance of major mergers over accretion dominated growth. We follow the formation of a “Draco” sized dSph halo of mass $10^8 M_{\odot}$ with several million particles and high force accuracy. Its internal structure and substructure resembles that of galactic or cluster mass halos: the density profile has a singular central cusp and it contains thousands of sub-halos orbiting within its virial radius demonstrating a self-similar nature to collisionless dark matter sub-clustering. The singular cores of substructure halos always survive complete tidal disruption although mass loss is continuous and rapid. Extrapolating wildly to earth mass halos with velocity dispersion of 1 m s^{-1} (roughly equal to the free streaming scale for neutralinos) we find that most of the dark matter may remain attached to bound subhalos. Further numerical and analytic work is required to confirm the existence of a detectable smooth component.

PACS number(s): 95.35.+d, 98.35.Gi, 98.35.Df, 98.35.Mp, 95.75.Pq

I. INTRODUCTION

Revealing the nature of dark matter is fundamental to cosmology and particle physics. A combination of observations and theory suggests that the dark matter consists of non-baryonic particles and in the large class of hierarchical cosmogonic models, a universe with a matter density dominated by cold dark matter (CDM) remains plausible albeit with some potential problems on small scales (c.f., Refs. [1–6]).

The only convincing method for confirming the existence and nature of dark matter is by direct detection. There are two prime candidate particles. Neutralinos are the lightest super-symmetric particles, otherwise known as WIMPS (weakly interacting massive particles). These can be identified in a laboratory by looking for phonons or a temperature increase from elastic scattering and nuclei recoil in various materials. Neutralinos also have a small cross-section for annihilation into decay prod-

ucts such as high energy photons or neutrinos that may be identified indirectly as a diffuse background from the galactic halo [7]. Axions are another type of hypothetical particle that have the additional motivation of ensuring that the strong interaction conserves charge-parity; these can be identified by stimulating their conversion to photons within a magnetic cavity (c.f., Ref. [8]).

Many laboratory and some space based experiments utilising these detection methods are in progress and after a great deal of technological development they are beginning to probe the parameter space allowed by cosmological and particle physics constraints (e.g. Refs. [9–12]). These experiments are all highly sensitive to the local density of particles and their velocity distribution [13–16]. The flux of gamma-rays on Earth from neutralino annihilations in the galactic halo is also very sensitive to any substructure in the dark matter [17]. It is therefore crucial to understand the phase space structure of galactic halos in the hierarchical CDM model in order that experiments can be fine tuned to search for the appropriate signals and that potential signals can be interpreted.

Many of the ongoing direct detection experiments

*Email:ben.moore@durham.ac.uk

adopt the principle that CDM particles passing near Earth have a smooth continuous density distribution with an isotropic Maxwellian velocity distribution with 3-d dispersion $\sim 270 \text{ km s}^{-1}$. We shall demonstrate that these assumptions are incorrect. Recent theoretical work has examined the possibility of velocity anisotropies resulting from halo rotation [18] or triaxiality [19,20]. Other halo models have also been studied e.g., Ref. [21], who assumes axially symmetric and cold collapse of matter to infer the presence of caustic rings in the solar neighbourhood. However, two decades of cosmological simulations of the cold dark matter model has clearly demonstrated that dark matter halos form via a series of mergers and accretions of dark matter clumps along highly filamentary mass distributions. Assuming symmetry and locally cold flows is an incorrect over-simplification of the true hierarchical growth [22].

At a given point in a CDM halo, the “smooth” dark matter background arises from material that has been tidally stripped from less massive halos (e.g., Ref. [23]). The velocity distribution of particles reflects the mass distribution of progenitor halos that have merged and accreted into the final system. The power spectrum of fluctuations in the CDM model allows small dense dark matter halos to collapse at very early epochs. The cut-off scale from the free streaming of neutralinos is approximately $10^{-12} M_{\odot}$ [24], although it is possible that the QCD transition may introduce features in the power spectrum that allow clumping of CDM on even smaller scales [25].

Previous simulations of the non-linear growth of halos systematically found triaxial structures with a smooth internal structure [26]. It was thought that the merging and virialisation process would naturally destroy the precursor halos, erasing the substructure and any memory of the initial conditions [27]. However, the over-merging of dark matter substructure halos was due primarily to poor force and mass resolution [28]. After several decades of code development, matched with increased hardware performance, numerical simulations have finally achieved a resolution of sub-kpc scales within a cosmological context. Recent high resolution numerical simulations can follow the evolution and survival of dark matter substructure halos (subhalos) as they orbit within dense environments [4,23,29].

We have previously used numerical simulations to investigate the structure of dark matter halos across a range of mass scales from $10^{12} M_{\odot}$ to $10^{15} M_{\odot}$. Rather than run many simulations at low resolution we have simulated several at the highest resolution possible with current technology. One of the key results that we have found is that substructure within hierarchical models is nearly scale free. The distribution and orbital properties of “halos-within-halos” is independent of halo mass - CDM galaxy halos contain literally thousands of halos more massive than those that surround the dwarf satellite galaxies in our own halo, Draco and Ursa-Minor [30,31]. In this paper we explore the phase space distribution of

CDM within galactic and sub-galactic halos addressing questions of direct relevance to the direct detection of dark matter. Given our limited resolution compared to laboratory scales, we discuss the extrapolation of our results to earth mass and solar system scales.

Section II discusses the simulation techniques and results of a high resolution simulation of the Local Group and a dark matter mini-halo. Section III discusses the observational constraints on the dark matter halo surrounding the Milky Way in the context of the CDM hierarchical model. Sections IV and V examine the survival of dark matter substructure and the velocity distribution of dark matter at the sun’s position within the Galactic halo. Section VI summarises the main results of this paper.

II. A COSMOLOGICAL SIMULATION OF THE LOCAL GROUP

Initially we perform a simulation of a 50 Mpc cube of a standard CDM universe with $\Omega_{CDM} = 1$, normalised such that $\sigma_8 = 0.7$ and the shape parameter $\Gamma = 0.5$ (a Hubble constant of $100 \text{ km s}^{-1} \text{ Mpc}^{-1}$ is adopted throughout). Although we use simulations within the context of the standard cold dark matter model, our results do not depend sensitively on the mass density of CDM or on the presence of a cosmological constant. The parent simulation contains 144^3 particles with a mass of $1 \times 10^{10} M_{\odot}$ and we use a force softening of 30 kpc. This is adequate for resolving the location and global properties of Galactic mass dark matter halos. The particle distribution is evolved using the extensively tested parallel treecode, “PKDGRAV”, that has accurate force resolution, periodic boundaries and variable timesteps. The code uses a co-moving spline softening length such that the force is completely Newtonian at twice our quoted softening lengths.

At a redshift $z=0$ we search for a pair of dark matter halos with similar dynamical properties as the Local Group, including mass, separation, infall velocity and proximity to a large Virgo-like cluster. The cosmological volume contains many binary halos of similar mass as the Local Group, but only a few that are in a similar dynamical state [32]. The particles that define one of the low resolution Local Group candidates (those particles within twice the virial radii of both dark matter halos) are traced back to a redshift $z=100$ to identify a volume that collapses into the final system. Within this arbitrary shaped region we extrapolate the power spectrum to smaller scales, matched at the boundaries such that both the power and waves of the new density field are identical in the region of overlap. This region is populated with a new subset of less massive particles and zones of heavier particles are placed outside this region, which allows the correct tidal field to be modelled from the entire cosmological volume of the initial box.

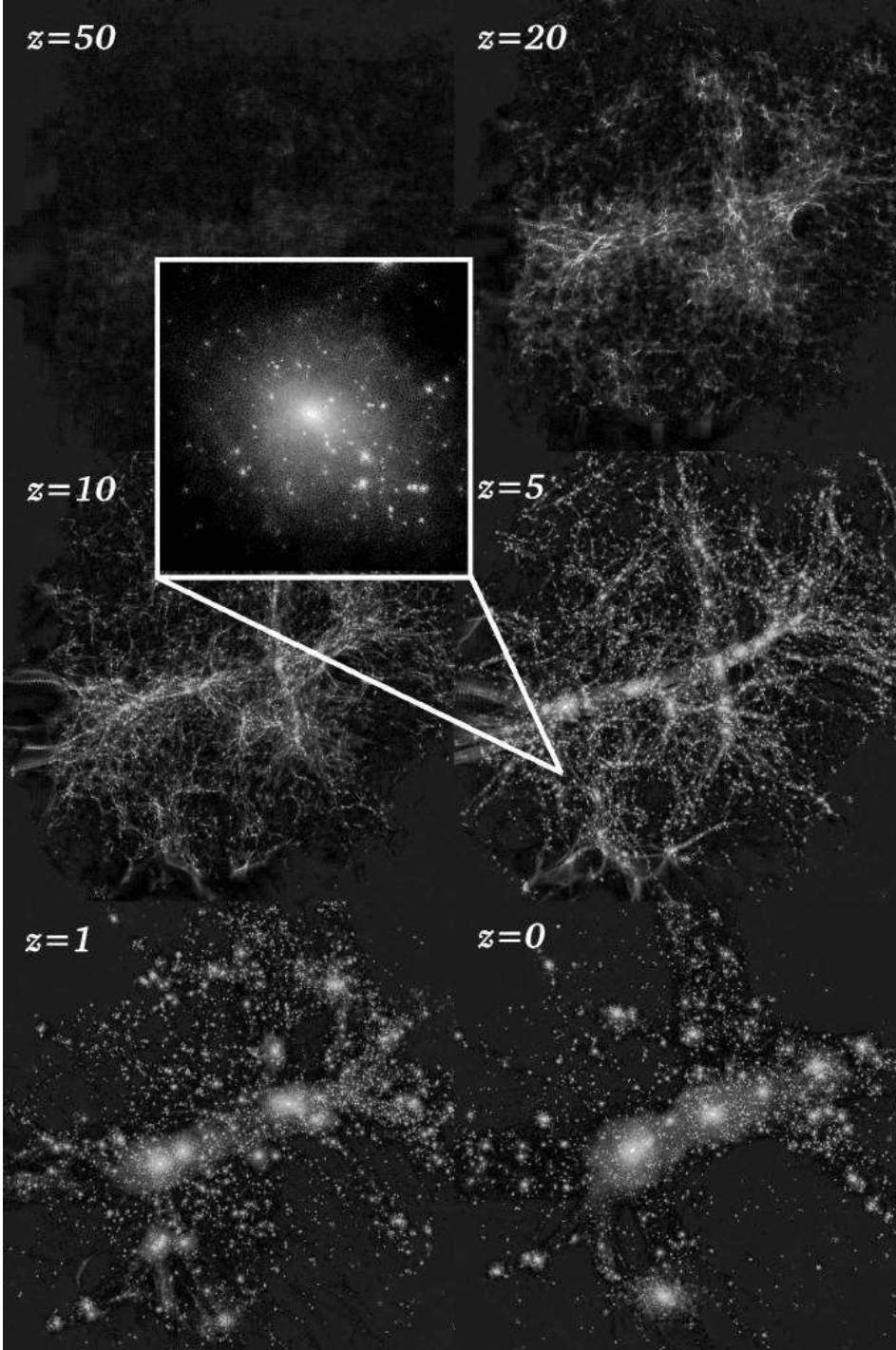


FIG. 1. The hierarchical formation of a “Local Group” within a cold dark matter universe. The grey scale shows the local density of dark matter at the indicated redshifts. At a redshift $z = 0$ we have two dark matter halos separated by 1 Mpc infalling at $\approx 100 \text{ km s}^{-1}$ with circular velocities $\approx 200 \text{ km s}^{-1}$. The inset box at $z=5$ shows the internal structure of a dark matter subhalo with total mass $10^8 M_\odot$. The region that collapses into this object was followed at a higher resolution such more than that 10^6 particles lie within its virial radius of 2 kpc. (The size of each panel is 4 comoving Mpc and the inset panel is 4 kpc.)

The particle mass in the high resolution regions is $1 \times 10^6 M_\odot$ and the spline force softening is set to 0.5 kpc. The starting redshift is increased such that the initial fluctuations are less than one percent of the mean density and we then re-run the simulation to the present epoch. This calculation required $\sim 150,000$ T3E cpu hours to evolve to the present day. The particles on the shortest timestep require more than 100,000 individual steps and in total we calculated $\sim 10^{15}$ floating point operations. The final virial radii and locations of the halos agree with those in the lower resolution simulation to within a few percent. (For reference, the accuracy parameters we use with PKDGRAV are $\theta(z > 2) = 0.5$, $\theta(z < 2) = 0.7$, $\epsilon = 0.2$.) At the final time, each halo contains $\sim 2 \times 10^6$ particles and is well resolved at a distance of 1% of the virial radius, $r_{vir} \approx 200$ kpc. Snapshots of the formation of this pair of halos is shown in Fig. 1 and their spherically averaged density profiles are plotted in Fig. 2.

A good fit to the density profiles of CDM Galactic halos is given by $\rho(r) \propto 1/[(r/r_s)^{1.5} + (r/r_s)^3]$ where the scale length $r_s = r_{vir}/c_{moore}$ and the concentration $c_{moore} \approx 0.67c_{nfw}$. Figure 2 shows the density profile expected in the concordance Λ CDM model in which the concentration is about a factor of two lower than the standard CDM model simulate here.

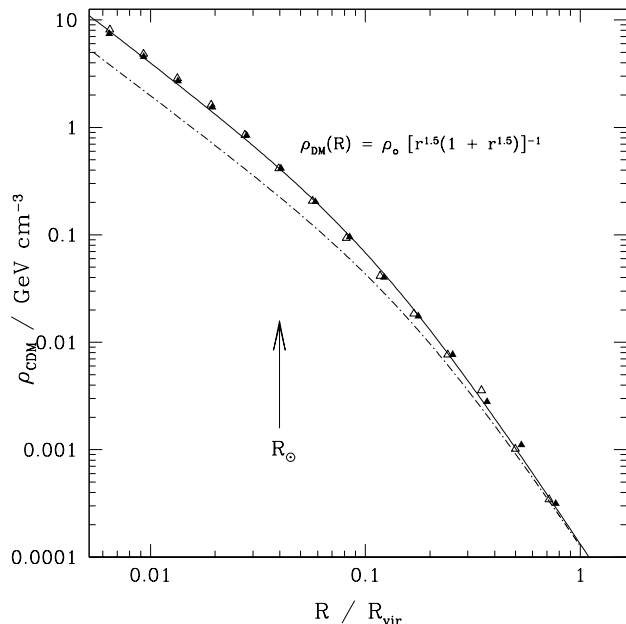


FIG. 2. The density profiles of the two high resolution “Local Group” CDM galactic halos. The density profiles of virialised equilibrium CDM halos are well fitted by the indicated curve, where $r = R/(R_{vir}/c_{moore})$. The density at the solar radius R_\odot depends on the cosmological model adopted, the standard CDM model simulated here would give values of $\rho_{CDM}(R_\odot)$ that are approximately a factor of two higher than a Λ dominated CDM model (dot-dashed curve).

A. The fractal nature of dark matter

The smallest scale on which we have evidence for dark matter is within the dwarf spheroidal satellites that orbit within the Galactic halo. Our Local Group simulation contains over 2000 of these systems with peak circular velocities, v_{peak} , larger than 10 km s^{-1} and most of these orbit within the virial radius of the two large halos. At our current resolution, most of the subhalos are smooth i.e. “halos within halos within halos” are found only within the largest substructures. If we could increase the resolution to 10^{10} particles we could accurately study the internal structure of dark matter subhalos and investigate the clustering of matter on very small scales. Such a simulation is probably about a decade away, therefore we shall repeat the “volume renormalization” process described above on a single dark matter subhalo from the Local Group simulation.

First we identify a dark matter mini-halo with a velocity dispersion of 10 km s^{-1} that accretes into one of the Local Group binary halos at a late epoch, $z \approx 3$. This halo would resemble the dark matter dominated dwarf spheroidal galaxies that orbit within the Galactic halo. The particles from the low resolution halo are traced back to their starting positions to identify the region to be re-simulated at higher resolution. We start this re-simulation at a redshift $z=150$ and our particle mass is $50M_\odot$ and our force softening is 10 parsecs – we can resolve dark matter halos collapsing at redshifts $z = 50$ with characteristic velocities $v_{circ} \lesssim 1 \text{ km s}^{-1}$. The “Draco” mass halo collapses/virialises at a redshift $z = 7$ and by $z = 3$ we have to stop the simulation since it becomes contaminated with heavy particles from the bounding regions as it enters the less well resolved galactic mass halo.

The blown up region in Fig. 1 shows the mass distribution within the virialised extent of the Draco halo at $z = 5$. At this epoch the mini-halo has a mass of $10^8 M_\odot$, circular velocity of 15 km s^{-1} and virial radius of 2 kpc in physical coordinates. Roughly 10% of its mass is attached to over 600 dark matter substructure halos containing more than 32 bound particles. The characteristic slope of the power spectrum on this scale is $n_{eff} \approx -2.9$ so that all mass scales are turning non-linear and collapsing at a similar time. In order for subhalos to survive, the timescale between collapse and accretion into a larger object must be sufficiently long to allow the halos to virialise and form dense cores. The density profiles of progenitor halos at $z=15$ shown in Fig. 3 demonstrate that they also have singular cuspy inner profiles.

Figure 3 shows the density profile of the Draco satellite at $z=4$. In physical coordinates the rotation curve peaks at 15 km s^{-1} at $r_{peak} = 1 \text{ kpc}$ and $r_{vir} = 3 \text{ kpc}$. We also plot the best fit Moore *et al.* [30] and NFW density profiles that have concentrations $c_{moore} = 3.5$ and $c_{nfw} = 5.2$. This latter value is close to that predicted by Navarro *et al.* [33] (NFW) scaling for an object of this mass $1.3 \times 10^8 M_\odot$ at this redshift. In fact, the NFW

scaling provides a good fit to the smallest well resolved progenitor halos with circular velocities $\sim 1 \text{ km s}^{-1}$ that also have cuspy singular density profiles (c.f., Ref. [34]). Figure 4 shows the circular velocity profile of the Draco halo as well as for two of its tiny subhalos and the fits shown in Fig. 3.

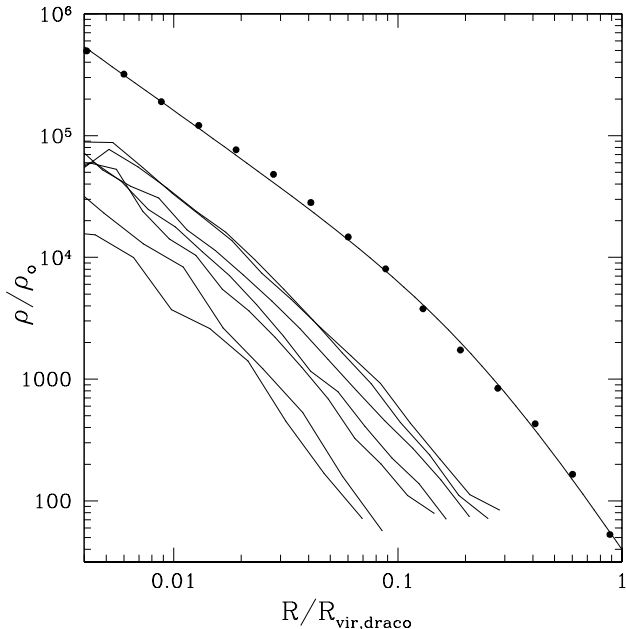


FIG. 3. The density profile of the “Draco” dark matter mini-halo at $z=4$ (dots) and seven randomly selected progenitor halos at $z=15$. The solid curve shows the best fit density profile to the Draco halo, constrained to have an outer slope of -3 but leaving the inner slope as a free parameter, resulting in a value of -1.3 .

We identify subhalos within the Draco halo using the same procedures as in Ref. [23]. The circular velocity function of subhalos within Draco, Galactic and Cluster mass CDM halos from the same cosmological model are compared in Fig. 5. The masses of these objects vary by 7 orders of magnitude yet they all contain similar amounts of dark matter substructure. The slope of the circular velocity function within the “Draco” halo, “Galaxy” halo and “Virgo” halos are $n(v_c) \propto v_c^{-\alpha}$ with $\alpha = 3.0, 3.7$ and 3.9 respectively.

The dark matter within virialised systems is nearly self-similar or fractal-like. The slope of the circular velocity function within the mini-halo is shallower than the galaxy and cluster halos which may reflect the fact that we are approaching the asymptotic “ $n=-3$ ” part of the power spectrum. (The amplitude of the curve is also lower, due in part to the redshift at which we are studying the halo – a halo of the same circular velocity today would have a virial radius 5 times larger.) We also caution that this halo has a very particular merger history that may not be typical of other halos of this mass.

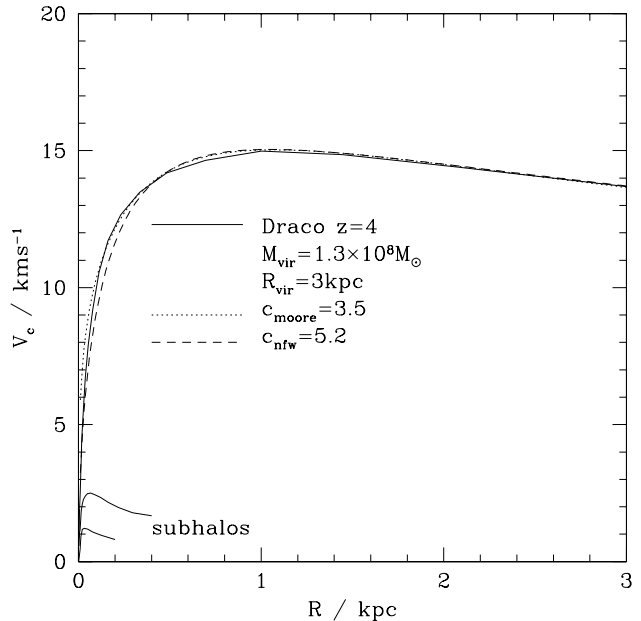


FIG. 4. The circular velocity curve of the “Draco” dark matter mini-halo at $z=4$ (solid curve). The dotted and dashed curves are the best fit Moore *et al.* and NFW density profiles respectively. The circular velocity curves of two small subhalos with circular velocities $\approx 1 \text{ km s}^{-1}$ are also plotted.

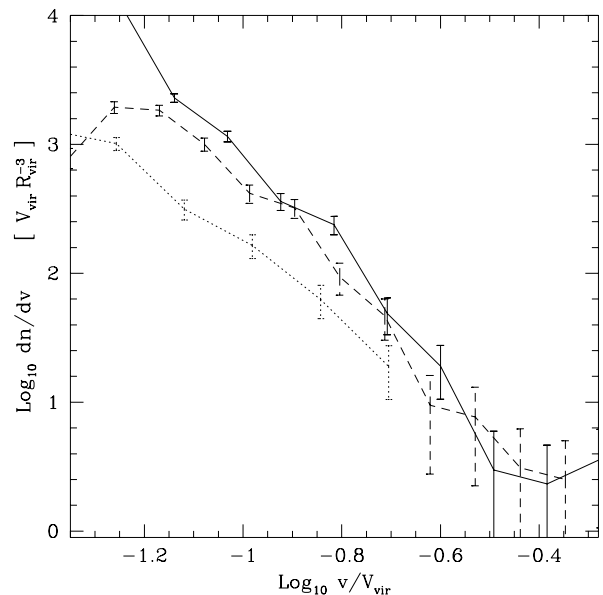


FIG. 5. The velocity distribution functions for dark matter subhalos within a CDM cluster, galaxy and mini-halo. Each halo has been simulated with $\gtrsim 10^6$ particles and using softening lengths $\lesssim 0.002 R_{vir}$. The peak velocities of the subhalos are normalised by the circular velocity at the virial radius of their parent halos.

III. THE MEAN DENSITY OF DARK MATTER AT R_\odot

The flux of particles through a detector depends on the local density of dark matter and the velocity distribution of particles relative to the earth’s motion through the galaxy [35]. Here we combine several observational constraints on the baryonic distribution within the Milky Way with our numerical simulations of halo structure to determine the possible range of CDM halos that may surround the Galaxy.

The density profile of CDM halos within a specific cosmology follow a single parameter family uniquely determined by their mass. The cosmological scatter of halo concentrations is about 30% for virialised halos not undergoing current mergers [33,36]. This scatter is largely due to variations in the virial radius at a fixed circular velocity and is sensitive to the presence of large substructure halos. If we consider just the structure internal to v_{peak} then deviations from our density profile are only of the order 10% (c.f. Figure 1 of Ref. [30]). The scatter in central density profiles is small because this region is completely relaxed and rarely contains substructure halos.

A. Upper limit

A single observed value of the circular velocity is insufficient to constrain the properties of the Galactic CDM halo, although the most important quantity to measure is the circular velocity at the sun’s position. Unfortunately, the structural properties of the Galaxy are not well known, *e.g.* the solar position $7 < R_\odot/\text{kpc} < 8.5$, the disk scale length $2 < r_d/\text{kpc} < 4$, the local circular velocity $190 < v_\odot/\text{kms}^{-1} < 230$ [37]. The maximum density of CDM at R_\odot can be determined by calculating the minimum contribution to v_\odot from the combined baryonic components.

The mass of an exponential disk is $M_d = 2\pi r_d^2 \Sigma(R_\odot) e^{R_\odot/r_d}$ where $\Sigma(R_\odot)$ is the vertical column density of baryons at the solar position R_\odot . Direct observations of the local stellar and gaseous distributions or dynamical estimates of the gravitating mass in the disk yield values of $\Sigma(R_\odot)$ lie in the range $40\text{--}90 M_\odot/\text{pc}^2$ [38–41]. Thus the baryonic disk mass lies in the range $4\text{--}8 \times 10^{10} M_\odot$, of which 67% lies within R_\odot . The Galactic bulge contributes a further mass of $1\text{--}2 \times 10^{10} M_\odot$ [42].

How does this compare to independent measurements? In order to explain the microlensing optical depth of K-giant stars towards the Galactic bulge, the stellar mass within R_\odot must be $> 7.6 \times 10^{10} M_\odot$ [43]. This is close to the mass of stars that a maximum disk allows and may be evidence that the Milky Way is a barred galaxy [44]. A further constraint on the central dark matter density can be derived using the kinematics of barred galaxies.

The existence of rapidly rotating bars and the strength and position of shocks in their gas flows, both indicate low central dark matter densities [45,46]. The analyses of these authors constrain the ratio $(v_{disk}/v_{halo})^2 > 2$ measured at $2r_d$ at the 2σ level. Applying these constraints to the Milky Way with $v_\odot = 220 \text{ km s}^{-1}$ and $v_{bulge}(R_\odot) = 70 \text{ km s}^{-1}$, implies circular velocities at $2r_d$ of $v_{halo} < 120 \text{ km s}^{-1}$ and $v_{disk} > 170 \text{ km s}^{-1}$. These parameters for the disk lie in the range discussed above and are illustrated in Fig. 6 as our fiducial Galactic model.

Summarising these constraints allows us to estimate the maximum mass of dark matter within R_\odot , given that we do not want to overestimate the contribution to the observed circular velocity. This gives $M_{CDM} \lesssim 3 \times 10^{10} M_\odot$ for $v_\odot = 220 \text{ km s}^{-1}$. Adopting the currently favoured Λ CDM model with $\Omega_\Lambda = 0.7$, $\Omega_{CDM} = 0.3$, $\sigma_8 = 0.9$, $h = 0.65$ constrains the structure of the maximum CDM halo to be; $c_{moore} = 6$ ($c_{nfw} = 9$), $v_{peak} = 153 \text{ km s}^{-1}$, $R_{vir} = 250 \text{ kpc}$, $v_{vir} = 124 \text{ km s}^{-1}$, $M_{vir} = 9 \times 10^{11} M_\odot$, $R(v_{peak}) = 52 \text{ kpc}$. Using the halo density profile defined in Section II we find a mean density of dark matter $\rho_{CDM}(R_\odot) \lesssim 0.23 \text{ (GeV cm}^{-3}\text{)}$. (Adopting an NFW profile with inner cusp of -1 would lower this value by about 15%.) For $v_\odot = 230 \text{ km s}^{-1}$ this density could rise by 30% to $\rho_{CDM}(R_\odot) = 0.3 \text{ (GeV cm}^{-3}\text{)}$.

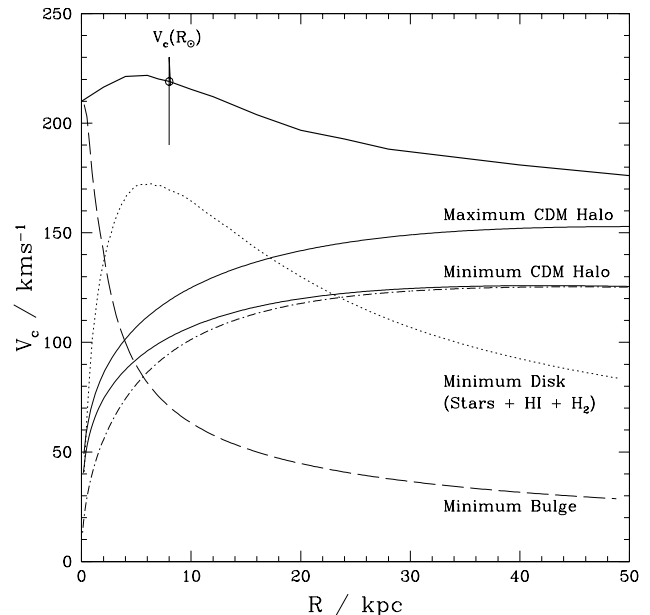


FIG. 6. The dashed and dotted curves show the minimum contribution to the Galactic circular velocity curve from bulge and disk components respectively. The solid curves show the minimum and maximum allowed CDM halos with central density cusp $\rho(r) \propto r^{-1.5}$. The upper thick solid curve is the total circular velocity profile of the Galaxy for the case in which the CDM halo is the maximum allowed by observational constraints. The minimum CDM halo is the least massive halo that can cool the observed mass of baryons within a Hubble time. The dot-dashed curve is a minimum “NFW” halo with central cusp $\rho(r) \propto r^{-1}$.

B. Lower limit

A lower limit to the mass of the Galactic halo can be found assuming that it must be massive enough to “cool” the observed quantity of baryons to form the visible galaxy [47,48]. This assumes that those baryons initially outside r_{vir} have not had time to cool and reach the central disk. This is probably an underestimate of the halo mass since a large fraction of the baryons may be external to the disk in a warm component – perhaps ejected via super novae feedback which is an essential ingredient to galaxy formation in the CDM model.

To estimate a lower limit to the halo mass we take a baryon fraction given by the upper limit from nucleosynthesis, $\Omega_b = 0.019h^{-2}$ [49] and a low Hubble constant $h = 0.6$. For a total baryonic mass of $8 \times 10^{10} M_\odot$, the halo mass must be $M_{vir} > (\Omega_o/\Omega_b)M_{baryon} > 4.6 \times 10^{11} M_\odot$ in order to cool the observed amount of baryons. (This calculation limits the total amount of ejected baryons to be less than the mass that currently resides in the Galaxy.) Within our adopted Λ CDM model this minimum CDM halo would have a density profile with parameters; $c_{moore} = 6$, $R_{vir} = 200$ kpc, $v_{vir} = 100$ km s $^{-1}$, $v_{peak} = 125$ km s $^{-1}$, $R(v_{peak}) = 40$ kpc and $M_{vir} = 4.6 \times 10^{11} M_\odot$. This leads to a lower limit of $\rho_{CDM}(R_\odot) \gtrsim 0.18$ (GeV cm $^{-3}$).

Although the Galactic CDM halo is tightly constrained we find that a Λ CDM halo is compatible with the observational constraints. Our fiducial Galactic model is also consistent with the total mass inferred from the orbits of its satellites [50] and the value of the circular velocity $v_c(50\text{kpc}) \approx 200$ km s $^{-1}$ found from modelling the Sagittarius tidal stream [51]. Detailed modelling of the thickness of the Galactic gas disk provides another constraint on the local dark matter density [52]. Finally, we note that it remains to be resolved whether or not the adiabatic contraction from the cooling baryons would increase the central CDM density beyond that allowed by the observations [53].

IV. STRUCTURE IN DENSITY SPACE

The previous calculation of the dark matter density assumes that the particles are smoothly distributed. If the dark matter is physically clustered on small scales then this estimate could radically change. For example, if the first objects that collapse in the CDM hierarchy are small and dense enough, they will survive the Galaxy’s tidal field and remain bound. The chances of the earth moving through one of these clumps may be so small that direct detection would not succeed. Here we discuss the tidally limited structure of CDM halos within halos.

The first numerical studies of collisionless dark matter halo collapses were carried out by Peebles [54] and White [26]. Although the final virialised structure had global mass and size comparable to observed structures, all

traces of substructure had vanished. Named the “overmerging” problem, small dark matter structures were initially resolved in the simulations but disrupted as soon as they merged into a more massive structure. This turned out to be a resolution problem [28], and as demonstrated in Section II, we can now resolve many thousands of dark matter substructure halos orbiting within the virialised extent of Galactic and sub-Galactic halos.



FIG. 7. The evolution of a dark matter subhalo orbiting on a circular polar orbit within a Galactic potential at 20 kpc. The snapshot is after 3 Gyrs, about 5 orbits. The tidal streams of dark matter lead and trail the surviving dark matter clump of which just 0.3 percent of the initial mass remains bound.

However, even our highest resolution simulations show little substructure within about 10% of the virial radius. This is primarily a resolution effect since we do not have enough particles to resolve the cores of tidally stripped halos. CDM halos have singular cuspy profiles on all mass scales simulated to-date from $10^6 M_\odot$ to $10^{15} M_\odot$, therefore a central core will always survive but would require extremely high mass resolution to resolve it.

If the number density of subhalos continues as a power law to very small masses would we expect a smooth component of matter at the solar radius? This question is quite subtle since the surviving fraction of halos at a given radius depends also on how the parent halo is assembled. i.e. is the formation dominated by major (similar mass) mergers or by accretion driven growth? In the former case halos will always be smooth since the halo centers coalesce to form a single system. In the latter case, halo cores always survive but may not have much mass attached to them. Further simulations and analytic modeling are required to fully address this question, here we make an estimate of the radius at which accreted subhalos can retain most of their mass intact

from the Galactic tidal field.

Although it is physically impossible to completely disrupt a CDM subhalo, once the tidal radius, r_t , imposed by the Galaxy approaches the radius at which the density profile becomes shallower than -2 , the subhalo loses mass rapidly. If $r_t > r_{peak}$ then the halo will be stable and lose very little mass. This behaviour can be understood in terms of the energy distribution of particles compared with the escape velocity at different radii. This process is illustrated in Fig. 7 in which we examine tidal mass loss for the extreme case. We construct an equilibrium dark matter halo with a peak circular velocity of 10 km s^{-1} using 10^7 particles, force softening of 10 parsecs and isotropic particle orbits. The model is an equilibrium Hernquist profile that has an inner density profile $\rho(r) \propto r^{-1}$ and is essentially a equilibrium replica of the Draco halo simulated earlier.

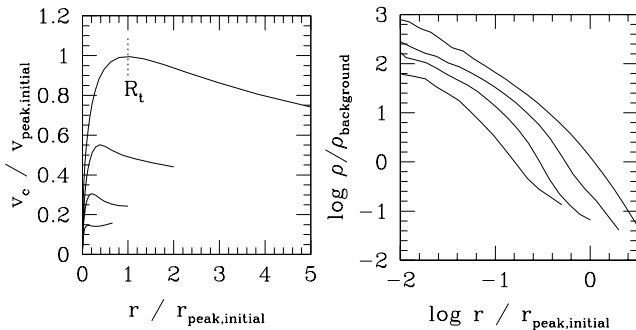


FIG. 8. The evolution of the circular velocity and density profiles of the satellite shown in Fig. 7. The curves show the initial configuration and subsequent times of 1, 2 and 3 Gyrs. The satellite is on a circular orbit at 20 kpc from the center of a Galactic potential and the theoretical tidal radius for this orbit is indicated.

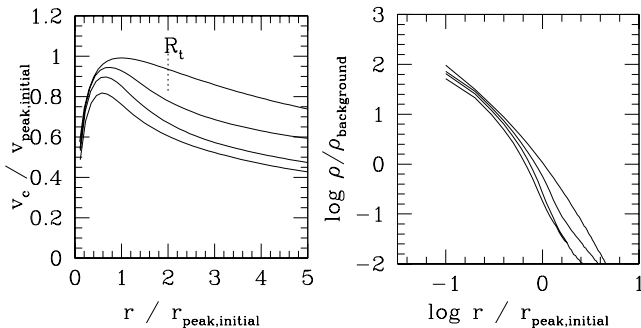


FIG. 9. The evolution of the circular velocity and density profiles of the satellite shown in Fig. 7. The curves show the initial configuration and subsequent times of 1, 2 and 3 Gyrs. The satellite is on a circular orbit at 40 kpc from the center of a Galactic potential.

Figure 7 shows the evolution of this model placed on a circular orbit within a Galactic potential for three billion years. The model has been constructed such that the tidal radius imposed by the Milky Way is equal to

the radius at which the satellite’s circular velocity peaks (this is the position at which the density profile becomes shallower than $\rho(r) \propto r^{-2}$). Most of the mass has been stripped away by tidal forces and now lies in two symmetric tidal tails of material that completely wrap around the entire orbit. In Fig. 8 we plot the evolution of the circular velocity curve and density profile of this satellite.

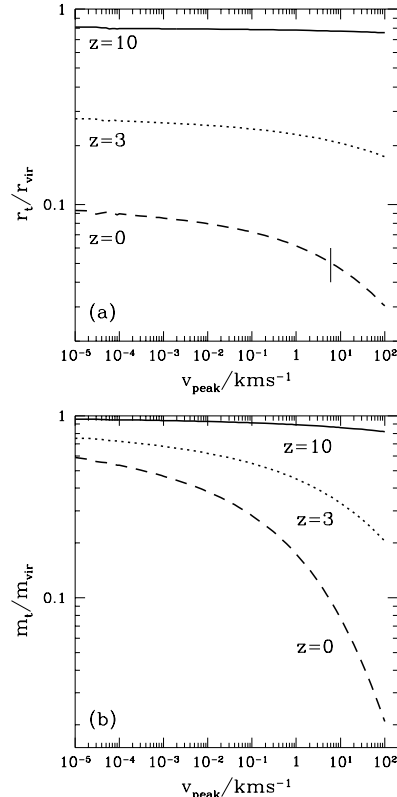


FIG. 10. The upper panel shows the ratio of tidal radius to virial radius for CDM subhalos of a given peak circular velocity orbiting at a distance of $R_\odot = 8 \text{ kpc}$ from the center of a $10^{12} M_\odot$ CDM halo. We consider satellites with concentrations scaling from the fiducial Λ CDM model with structural parameters defined at three different redshifts. We plot results down to halos with characteristic velocity of 1 cm s^{-1} which is roughly the free streaming limit for neutralinos. The lower panel shows the ratio of remaining bound mass to the initial virial masses of the subhalos. If subhalos enter Galactic progenitor halos at $z=10$ then more than 90% of their mass remains bound.

The mass loss is continuous as particles on radial orbits escape, which in turn decreases the tidal radius allowing more particles to escape. Fig 9 shows the same satellite orbiting at 40 kpc within the same potential. In this case the tidal radius imposed by the Galaxy is twice as large and lies beyond the inner core causing the satellite to lose mass less rapidly. Whereas previously we found that after 3 Gyrs only 0.3% of the initial mass remains bound, in this case 40% remains bound at the final time.

Applying these results to subhalos orbiting within the Milky Way allows us to estimate a radius at which a halo of a given concentration will loose most of its mass to the smooth background, i.e. the radius at which the Galactic tidal field truncates the satellite at $r(v_{peak})$. The ratio of r_{peak}/r_{vir} decreases with halo mass (halo concentration increases for small masses) therefore smaller mass halos can survive intact deeper within the Galactic potential. At the location of the earth within the Galactic halo we estimate that halos with circular velocities larger than $\approx 1 \text{ km s}^{-1}$ *accreting today* will lose more than 95% of their mass. Fig. 10 shows the tidal radii and masses of CDM subhalos orbiting on circular orbits at R_{\odot} with a CDM parent halo of mass $10^{12} M_{\odot}$. To calculate tidal radii we use the orbital resonance theory derived by Weinberg (1998) which is slightly more stringent than the standard technique of using equipotential surfaces. To make this calculation we have assumed that the concentration $c = r_{vir}/2r_{peak}$ scales with mass as predicted by NFW. Fig. 10 shows that the amount of tidally stripped mass depends sensitively on the redshift that subhalos accrete into the Milky Way.

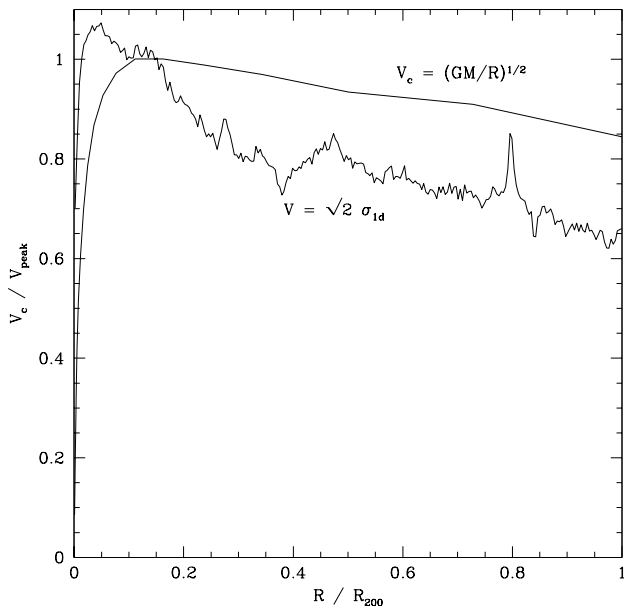


FIG. 11. The circular velocity profile, ($v_c = \sqrt{GM/R}$), and one dimensional velocity dispersion profile (multiplied by $\sqrt{2}$) of one of the Local Group halos from Section 2.

V. STRUCTURE IN VELOCITY SPACE

The fraction of mass in the smooth component could vary from 0% to 100% depending solely on the subhalo structure, let alone the formation history of the central Galactic halo. If the halo is predominantly smooth at R_{\odot} , as our current resolution limited simulations find, then what can we learn by examining the velocity distri-

bution of dark matter particles?

A. The global velocity dispersion profile

We show the spherically averaged circular velocity, $v_c = \sqrt{GM/r}$, in Fig. 11 along with the actual 1d velocity dispersion of particles averaged in shells. The velocity dispersion profile of Galactic mass halos peaks sharply at about 3–7% of the virial radius (approximately R_{\odot}) and falls to a value of $\approx \sigma_{peak}/2$ at the halo center and virial radius.

B. Anisotropy parameter

Direct detection experiments are sensitive to the energy spectrum of dark matter particles arriving on the earth. Some detectors, such as DRIFT, are also directionally sensitive to incoming WIMPS. The anisotropy parameter can be defined as $\beta(r) = 1 - \langle v_t \rangle^2 / \langle v_r \rangle^2$, where $\langle v_r \rangle$ and $\langle v_t \rangle$ are the mean radial and tangential velocities at radius r . Using this definition, isotropic, radial and circular orbits would have $\beta = 0, 1, < 0$ respectively.

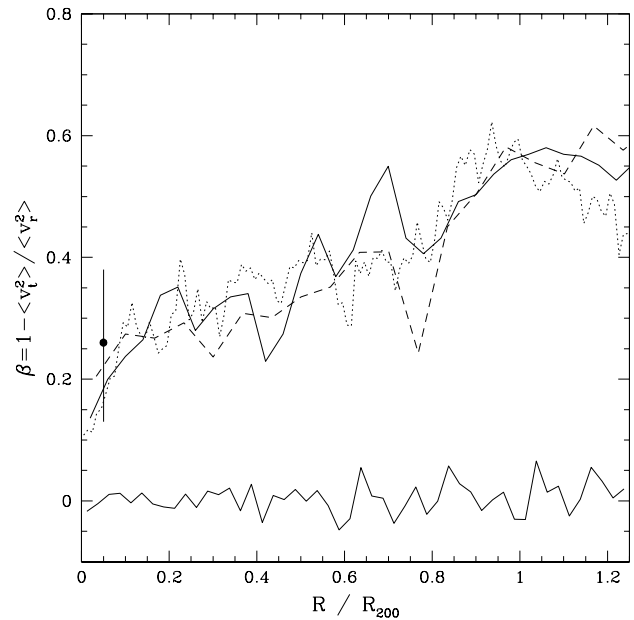


FIG. 12. The anisotropy parameter β is plotted to the virial radii for a halo simulated at three different resolutions: dashed, solid and dotted are low, intermediate and high resolution simulations of the same halo. The lower solid curve with $\beta \approx 0$ is a smooth halo constructed with similar structural parameters as the intermediate resolution CDM halo but with all particles on isotropic orbits, illustrating the Poisson noise in this quantity. At the solar radius, $R_{\odot} \approx 0.5\% R_{vir}$ we can expect values of $\beta = 0.1 - 0.4$ from our limited set of six high resolution Galactic mass halos [5] denoted by the single filled circle with an error bar.

In Fig. 12 we plot the anisotropy parameter of a single CDM halo simulated with three different resolutions; $10^{4.3}$, $10^{5.8}$, $10^{6.7}$ particles within the virial radius and force resolution $< 0.01R_{vir}$. The value of β appears to be independent of resolution since we find the same (noisy) trend in each simulation. (We also found no change in shape as we increase the numerical resolution – the ratio of long:intermediate:short axis in these three runs are the same to within 20% at all radii.) The behaviour of this halo is typical of our simulations with β rising from about 0.2 at R_{\odot} to 0.8 at R_{vir} . The average value of $\beta \approx 0.26 \pm 0.1$ at $R_{\odot} = 5\%R_{vir}$ was found using the results of 6 high resolution CDM halos from Ref. [30].

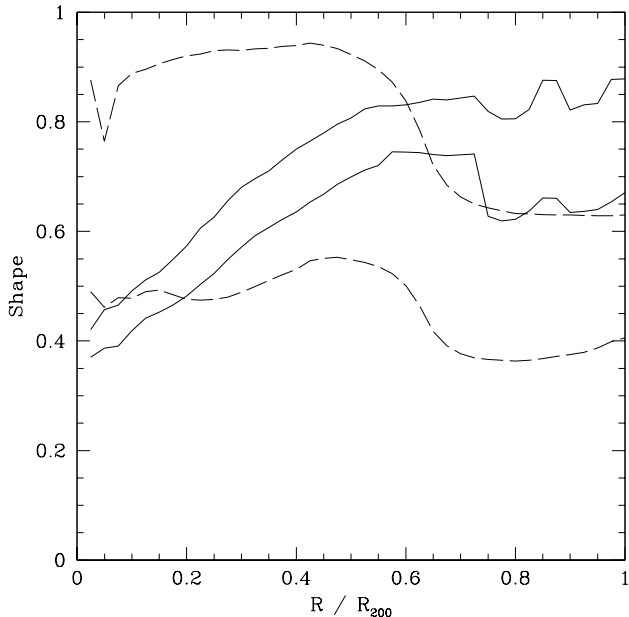


FIG. 13. The shapes of the two high resolution Local Group halos plotted out to their virial radii. The upper and lower curves for each halo show the intermediate:long and short:long axial ratios. One of the halos is prolate (solid curves) and is highly flattened in the center but becomes more spherical in the outer region. The other halo is oblate (dashed curves) but undergoes an abrupt shape change at about $0.5R_{vir}$ due to a major accretion event.

C. Anisotropy within triaxial halos

Figure 13 shows the axial ratios of the two Local Group halos as a function of radius. One of the halos (solid curves) is clearly prolate, with short to long axis ratio similar to the intermediate to long axis ratio. This halo is highly triaxial at the center but becomes more spherical towards the virial radius. The other halo (dashed curve) is oblate in the center becoming more prolate in the outer region. The origin of these shapes depend on the merger history of the halos – the oblate halo is particularly interesting since it suffers a major merger at

$z = 0.7$. This leads to an abrupt change in shape and angular momentum at $0.5r_{vir}$. Figure 14 shows how the angle of the angular momentum vector varies with radius from each of these halo centers. The angular momentum of shells varies with radius, wandering by $\gtrsim 100$ degrees from the center to the virial radius.

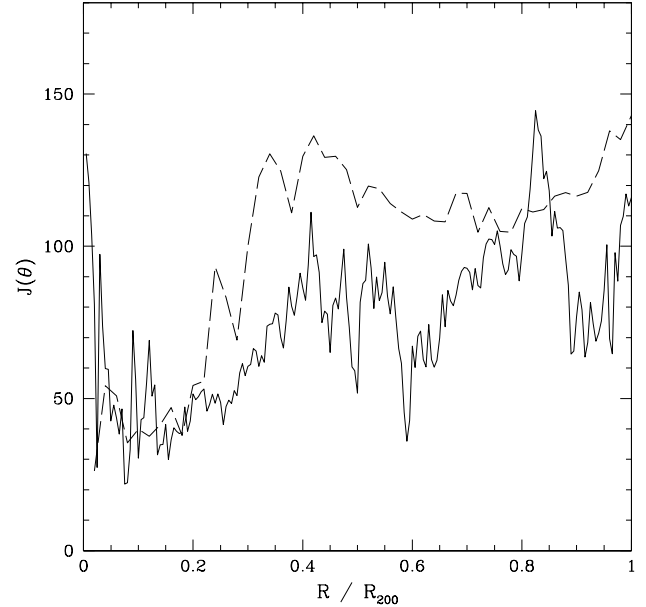


FIG. 14. The variation of the angular momentum vector as a function of radius of the two halos shown in Fig. 13. The direction of the vector for the prolate halo (solid curve) wanders by about 50 degrees whereas the oblate halo (dashed curve) changes sharply by 90 degrees close to the region where the shape of the density distribution changes.

CDM halos are clearly complex systems with complicated formation histories. They cannot be modelled as spherical or even simple triaxial structures with constant flattening or angular momentum but they do have a remarkable regularity in their phase space density profiles [55]. Although axially symmetric collapse of a cold rotating mass distribution may give rise to significant caustic features [21,56], this would not be a prediction of the CDM model.

If a halo is triaxial then the energy distribution of particles will provide the support for that shape (e.g., Ref. [20]). Here we study the central velocity structure of the prolate halo in more detail by sampling the particles in the small cubes indicated in Fig. 15. We find a mean value of $\beta = 0.36$ in the central 10% of the halo, whereas in positions L1 and L2, on the long axis, we find that the orbits are even more radially biased with $\beta = 0.45$. On the short axis the orbits are still radially biased however they are more circular than the mean with locations S3 and S4 having $\beta = 0.25$.

The distribution of particle velocities and speeds along the short and long axis are shown in Fig. 16. The height and width of the velocity distribution varies significantly

and a dark matter detector may find different event rates and signal profiles depending on its location. The differential rate for detecting CDM particles is simply

$$\frac{dR}{dQ} \propto \int_{v_{min}}^{\infty} \frac{f_r(v)}{v} dv$$

where R is the rate, Q is the recoil energy and $f_r(v)$ is the probability distribution of particle speeds relative to the detector [57]. In a forthcoming paper we will make predictions for event rates and modulation signals using the velocity distributions obtained directly from these halo simulations.

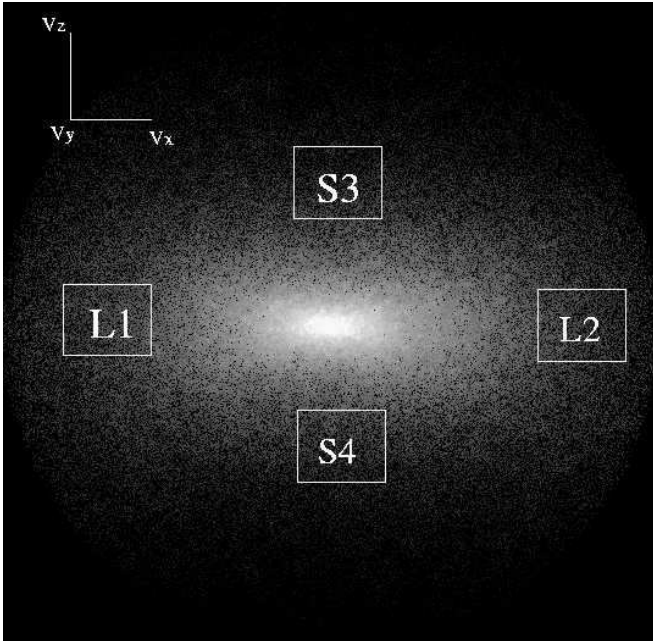


FIG. 15. The grey scale shows an edge on view of the particle distribution within the inner 10% of the prolate dark matter halo. The boxes indicate cubes that contain 2000 particles that we use to analyse the velocity anisotropy. L1 and L2 lie in the long axis of the density distribution whereas S3 and S4 lie in the short axis.

D. Dark matter streams

A halo that accretes a smaller mass satellite will tidally disrupt the satellite into tidal tails that slowly wrap in phase space (c.f., Ref. [58,16]). The symmetric tidal tails in Fig. 7 illustrated this process for a single high resolution satellite. The presence of dark matter streams may be inferred using directional dark matter detectors such as DRIFT, or by finding a highly peaked signal resulting from particles entering the detector with similar energies.

Numerical resolution sets a limit to the masses of the first clumps of dark matter that collapse within the CDM model. Most of the mass that has collapsed by $z=10$ ends up making the inner few percent of the final halo. The first clumps to collapse are extremely dense yet have

only a handful of particles - thus they have a smooth phase space structure that may be dominated by relaxation effects. In order to correctly follow the phase space structure at R_\odot it is necessary to correctly resolve the formation of the progenitor halos at $z = 10$. This would require a simulation with at least 10^{10} particles.

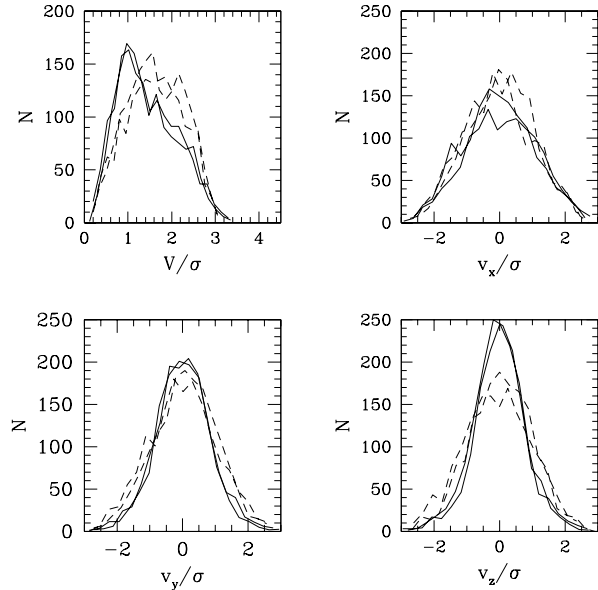


FIG. 16. The velocity histograms of particles taken from the regions indicated in Fig. 15. The solid and dashed curves are in the long and short axis respectively. The first panel uses the total velocity vector whereas the other three are just the v_x , v_y and v_z components. (The orientation of these vectors with respect to the density distribution are shown in Fig. 15.)

Figure 17 shows the velocity structure within one of the Local Group CDM halos sampled at three different radii - close to the solar radius, at half the virial radius and near the edge of the virial radius. The amount of structure in velocity space depends on where we sample the halo. In the outer region we find that all of the particles lie within several distinct streams with a velocity distribution that is remarkably non-Gaussian. At the halo center, the streams have phase wrapped several times and give rise to a smooth structure in velocity space.

The key question that we would like to answer is; *on a scale of order the size of the earths orbit around the sun, are we dominated by a single stream of dark matter, or by many thousands of overlapping streams?*

Our simulation shows that the phase space distribution is smooth at R_\odot . However we can only resolve subhalos as small as $10^8 M_\odot$ which have internal velocity dispersions of order 10 km s^{-1} and can phase wrap several times around the Galaxy in a Hubble time. Therefore in our patch of phase space that is 2kpc on a side, we find multiple streams from the same tidally disrupted halos.

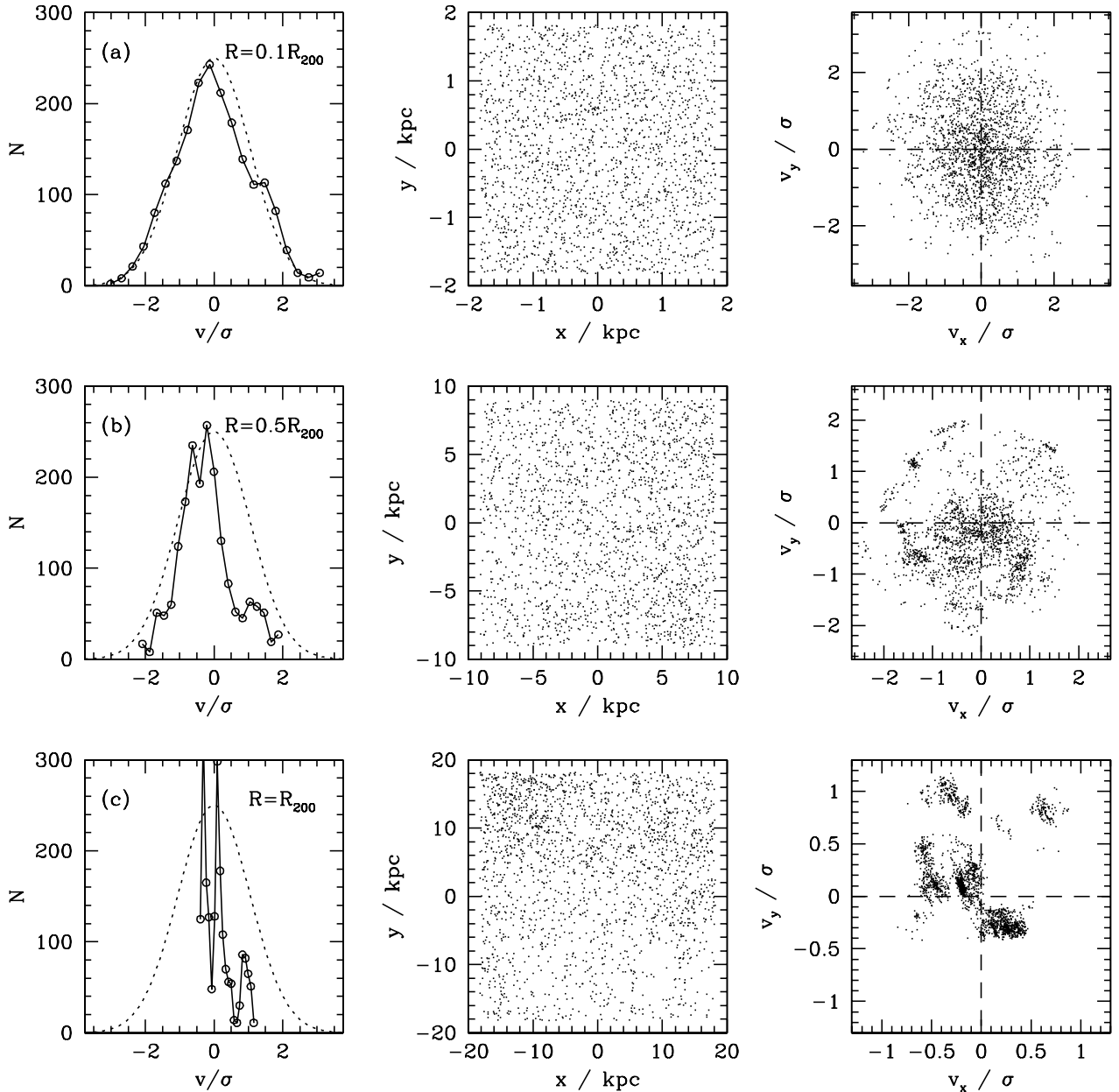


FIG. 17. The structure in velocity space as a function of position within the simulated Galactic halo. We have taken 3 cubes at different positions in the halo that are smooth in density space. Each cube contains about 1000 particles and has no bound subhalos within them as can be seen in the central panels. The left panel shows the histogram of one component of the distribution of particle speeds in each cube – the curve shows a Maxwellian distribution with velocity dispersion σ set equal to the spherically averaged value at $0.1R_{vir}$. The right panels show the x and y components of velocity plotted against each other.

If we had infinite resolution and examined a volume that was one parsec on a side what would we find? We would then be sensitive to the substructure within our poorly resolved $10^8 M_\odot$ halos.

A tiny CDM halo with $v_{peak} = 1 \text{ m s}^{-1}$ has $M_{vir} = 10^{-6} M_\odot$, $r_{vir} = 0.5$ parsecs, $r_{peak} = 0.001$ parsecs and

a concentration $c=400$ at a redshift $z=0$. Its tidal radius at R_\odot is $r_t = 0.05$ parsecs which encloses a mass of $10^{-7} M_\odot$. A straightforward simulation of this structure orbiting at R_\odot demonstrates that its tidal streams would be ≈ 50 parsecs long and 0.1 parsecs wide – certainly not phase wrapped. A halo with the same circu-

lar velocity at a redshift $z=10$ would have even smaller tidal streams. The mean mass density of CDM at R_\odot is $\sim 10^{-3}M_\odot/\text{pc}^3$, therefore if the central halo was made entirely from streams of tidally disrupted 1 m s^{-1} halos at $z=10$, we estimate that their filling factor is of order unity, with large uncertainties.

Future analytic work is clearly necessary to resolve these issues. However, it is possible that the density of dark matter in the solar system is zero, or that the solar system may be moving through a single stream of CDM particles that has bulk motion of $\approx 200\text{ km s}^{-1}$, with a velocity distribution of only a few m s^{-1} .

VI. CONCLUSIONS

We have carried out a high resolution numerical simulation of the Local Group and one of its substructure halos focussing our analysis on properties relevant to direct detection experiments. We summarise our main conclusions here:

- We combined our halo density profiles with observational constraints on the baryonic content of the Galaxy to infer the local density of dark matter. Observations favour a dominant baryonic component within $R_\odot = 8\text{ kpc}$ which leaves a CDM halo that contributes $\lesssim 3 \times 10^{10}M_\odot$ within the same radius. This constrains the local dark matter density to be $\rho(R_\odot) \lesssim 0.23\text{ GeV/cm}^3$ for a Galaxy with $v_\odot = 220\text{ km s}^{-1}$.

- CDM halos form via a series of many mergers and accretion events. The final triaxial halos have a complex structure; the shapes can vary from oblate to prolate and the angular momentum axis can change by more than 100 degrees in a single system. Axially symmetric collapse can not be applied to infer the structure of CDM halos – neither do we find or expect to find significant caustic features, such as rings or shells.

- We increased the resolution within a region that collapses to form a 10^8M_\odot halo that is typical of those that may surround the Galactic dwarf spheroidal galaxies. Even on this mass scale CDM halos have cuspy singular density profiles and contain a remarkable amount of surviving substructure – dwarf spheroidals resemble scaled versions of galaxies or clusters. The slope of the circular velocity function is steeper in higher mass halos, perhaps indicating a dependence on the slope of the power spectrum.

- The smallest dark matter halos that we can resolve, with circular velocities $\sim 1\text{ km s}^{-1}$, have cuspy singular density profiles and concentration parameters that scale as predicted by Navarro *et al.* [33].

- We show that halos with circular velocities $\lesssim 1\text{ km s}^{-1}$ can survive orbiting at the solar position within the Galactic potential. Since the central Galactic halo is in place by $z=10$, nearly all of the accreted halos will remain intact and retain most of their mass. The presence of a smooth component of dark matter at R_\odot depends on

the detailed merger history of the Galaxy and on the internal structure of the first CDM halos to collapse with characteristic velocities of $1\text{ m s}^{-1} - 1\text{ km s}^{-1}$.

- The orbits of the particles in the smooth component are radially biased – the spherically averaged anisotropy parameter at R_\odot may lie in the range $0.1 \lesssim \beta \lesssim 0.4$.

- The velocity distribution of CDM particles varies significantly with the location of the observer and cannot be approximated by a single Maxwellian.

- At our current resolution, the outer halo is made entirely from discrete streams of material originating from tidally stripped subhalos. Closer to the halo centre these streams have phased wrapped several times. Further analytic and numerical work is required to investigate the numbers of streams flowing through the solar system or the fraction of dark matter that is smoothly distributed on this scale.

ACKNOWLEDGEMENTS

Many thanks to Carlos Frenk, Amina Helmi, Adrian Jenkins, Luis Theodoro and Simon White for useful discussions. Ben Moore is supported by the Royal Society and acknowledges the Virgo Consortium for computing resources. Carlos Calcáneo-Roldán continues his research thanks to a grant from CONACyT (Mexico).

-
- [1] B. Moore, *Nature*, **370**, 620 (1994).
 - [2] R.A. Flores, and J. R. Primack, *Astrophys. J. Lett.* **457**, L5 (1994).
 - [3] A. Burkert, *Astrophys. J. Lett.*, **447**, L25 (1995).
 - [4] A. Klypin, A. V. Kravtsov, O. Valenzuela, and F. Prada, *Astrophys. J.* **522**, 82 (1999).
 - [5] B. Moore, S. Ghigna, F. Governato, G. Lake, T. Quinn, J. Stadel, and P. Tozzi, *Astrophys. J. Lett.* **524**, L19 (1999).
 - [6] J. A. Sellwood, *Astrophys. J.* **540**, L1 (2000).
 - [7] L. Bergström, *New Astron. Rev.*, **42**, 245 (1998).
 - [8] K. Griest, *Phys. Rev. Lett.* **61**, 666 (1988).
 - [9] M. J. Lehner, K. Griest, C. J. Martoff, G. E. Masek, T. Ohnuki, D. Snowden-Ifft and N. J. Spooner, *astro-ph/9905074*.
 - [10] R. Bernabei *et al.* [DAMA Collaboration], *Phys. Lett. B* **480**, 23 (2000).
 - [11] R. Abusaidi *et al.* [CDMS Collaboration], *Phys. Rev. Lett.* **84**, 5699 (2000).
 - [12] A. Benoit *et al.* [EDELWEISS Collaboration], *astro-ph/0106094*.
 - [13] C. J. Copi, and L. M. Krauss, *Phys. Rev. D.* **63** 043507 (2001).
 - [14] P. Ullio and M. Kamionkowski, *JHEP* **0103**, 049 (2001).
 - [15] L. M. Widrow, *Astrophys. J., Suppl. Ser.* **131**, 39 (2000).
 - [16] D. Stiff, L. M. Widrow, J. Frieman, *astro-ph/0106048*.

- [17] C. Calcáneo-Roldán, and B. Moore, *Phys. Rev. D.* **62** 123005 (2000).
- [18] M. Brhlik and L. Roszkowski, *Phys. Lett. B* **464**, 303 (1999)
- [19] M. Kamionkowski, and A. Kinkhabwala, *Phys. Rev. D.* **57**, 3256 (1998).
- [20] N. W. Evans, C. M. Carollo, C.M. and P. T. de Zeeuw, *Mon. Not. R. Astron. Soc.* **318**, 1131 (2000).
- [21] P. Sikivie, *Phys. Rev. D* **60**, 063501 (1999).
- [22] B. Moore, astro-ph/0103094.
- [23] S. Ghigna, B. Moore, F. Governato, G. Lake, T. Quinn, and J. Stadel, *Mon. Not. R. Astron. Soc.* **300**, 146 (1998).
- [24] D. J. Schwarz, and S. Hofmann, *Nucl. Phys. Proc. Suppl.* **87**, 93 (2000).
- [25] C. Schmid, D. J. Schwarz, and P. Widerin, *Phys. Rev. Lett.* **78**, 791 (1997).
- [26] S. D. M. White, *Mon. Not. R. Astron. Soc.* **177**, 717 (1976).
- [27] S. D. M. White and M. Rees, *Mon. Not. R. Astron. Soc.* **183**, 341 (1978).
- [28] B. Moore, N. Katz, and G. Lake, *Astrophys. J.* **457**, 455 (1996).
- [29] B. Moore, F. Governato, T. Quinn, J. Stadel, and G. Lake, *Astrophys. J.* **499**, L5 (1998).
- [30] B. Moore, T. Quinn, F. Governato, J. Stadel, and G. Lake *Mon. Not. R. Astron. Soc.* **310**, 1147 (1999).
- [31] A. Klypin, S. Gottlöber, A. Kravtsov, and M. Khokhlov, *Astrophys. J.* **516**, 530 (1999b).
- [32] F. Governato B. Moore, R. Cen, J. Stadel, G. Lake and T. Quinn *New Astron.* **2**, 91 (1997).
- [33] J. F. Navarro, C. S. Frenk, and S. D. M. White, *Astrophys. J.* **462**, 563 (1996).
- [34] H. Jang-Condell, and L. Hernquist, *Astrophys. J.* **548**, 68 (2001)
- [35] K. Freese, J. Frieman, and A. Gould, *Phys. Rev. D.* **37**, 3388 (1988).
- [36] V. R. Eke, J. F. Navarro, and M. Steinmetz, astro-ph/0012337.
- [37] P. D. Sackett, *Astrophys. J.* **483**, 103 (1997).
- [38] K. Kuijken K. and G. Gilmore G. *Astrophys. J. Lett.* **367**, L9 (1991).
- [39] C. Flynn, and B. Fuchs, *Mon. Not. R. Astron. Soc.* **270**, 471 (1994).
- [40] C. Flynn, A. Gould, and J. Bahcall, *Astron. Soc. Pac. Conf. Ser.* **165**, 387 (1999).
- [41] W. Dehnen, and J. Binney, *Mon. Not. R. Astron. Soc.* **298**, 387 (1998).
- [42] O. E. Gerhard, *Astron. Soc. Pac. Conf. Ser.* **182**, 307 (1999).
- [43] J. Binney, N. Bissantz, N., and O. Gerhard, *Astrophys. J. Lett.* **537** L99 (2000).
- [44] O. Gerhard, *Astron. Soc. Pac. Conf. Ser.* **197**, 201 (2000).
- [45] V. P. Debattista and J. A. Sellwood *Astrophys. J. Lett.* **493**, L5 (1998).
- [46] B. J. Weiner, J. A. Sellwood, and T. B. Williams, *Astrophys. J.* **546**, 931 (2001).
- [47] S. D. M. White, J. F. Navarro, A. E. Evrard, and C. S. Frenk, *Nature (London)* **366** 429 (1993).
- [48] J. F. Navarro, and M. Steinmetz, *Astrophys. J.* **528**, 607 (2000).
- [49] D. Tytler, S. Burles, L. Lu, X. Fan, A. Wolfe, and B. D. Savage, *Astron. J.* **117**, 63 (1999).
- [50] M. I. Wilkinson, and N. W. Evans, *Mon. Not. R. Astron. Soc.* **310**, 645 (1999).
- [51] R. Ibata, G. F. Lewis, M. Irwin, E. Totten, and T. Quinn, *Astrophys. J.* **551**, 294 (2001).
- [52] R. Olling, and M. R. Merrifield, astro-ph/0104465.
- [53] J. Barnes and S. D. M. White, *Mon. Not. R. Astron. Soc.* **211**, 753 (1984).
- [54] P. J. E. Peebles, *Astron. J.* **75**, 13 (1970).
- [55] J. E. Taylor, and J. F. Navarro, astro-ph/0104002.
- [56] A. M. Green, *Phys. Rev. D.* **63**, 103003 (2001).
- [57] G. Jungman, M. Kamionkowski, and K. Griest, *Phys. Rep.* **267**, 195 (1996).
- [58] A. Helmi, and S. D. M. White, *Mon. Not. R. Astron. Soc.* **307**, 495. (1999).